Original Article

Biodistribution and radiation dosimetry of multiple tracers on total-body positron emission tomography/computed tomography

Lianghua Li, Liangrong Wan, Haitao Zhao, Cheng Wang, Weijun Wei, Jianjun Liu

Department of Nuclear Medicine, Institute of Clinical Nuclear Medicine, Renji Hospital, School of Medicine, Shanghai Jiao Tong University, Shanghai, China

Contributions: (I) Conception and design: L Li, W Wei, J Liu; (II) Administrative support: L Wan, H Zhao, C Wang, J Liu; (III) Provision of study materials or patients: L Li, W Wei; (IV) Collection and assembly of data: L Li, L Wan, W Wei, J Liu; (V) Data analysis and interpretation: All authors; (VI) Manuscript writing: All authors; (VII) Final approval of manuscript: All authors.

Correspondence to: Prof. Weijun Wei, PhD; Prof. Jianjun Liu, PhD. Department of Nuclear Medicine, Renji Hospital, School of Medicine, Shanghai Jiao Tong University, 160 Pujian Road, Shanghai 200127, China. Email: wwei@shsmu.edu.cn; nuclearj@163.com.

Background: [^{18}F]F-FDG, [^{68}Ga]Ga-PSMA-11, and [^{68}Ga]Ga-FAPI-04 have achieved good results in multiple clinical trials and clinical practice, but the imaging of these tracers is limited to traditional short-axis positron emission tomography/computed tomography (PET/CT). Therefore, we aimed to use total-body PET/CT dynamic scanning to describe whole-body biodistribution of these three tracers and to calculate more precise radiation doses.

Methods: Total-body PET/CT (uExplorer, United Imaging Healthcare) dynamic scanning was performed on 54 patients, including 30 patients with [^{18}F]F-FDG, 10 patients with [^{68}Ga]Ga-PSMA-11, and 14 patients with [^{68}Ga]Ga-FAPI-04. A 60-minute dynamic scanning of whole body was performed simultaneously after bedside bolus injection of the corresponding tracers. The dynamic sequence of 92 frames was quantitatively analyzed by the Pmod4.0 software. Whole body biodistribution was calculated as time-activity curves (TACs) describing dynamic uptake patterns in the subject's major organs, followed by calculation of tracer kinetics and cumulative organ activity. Finally, combined with the OLINDA/EXM software, effective doses of the different tracers and individual organ doses were calculated.

Results: In a systematic TAC analysis of three tracers, we identified distinct biodistribution patterns in major organs. [^{68}Ga]Ga-PSMA-11 showed a trend of rapid increasing and slow decreasing in liver, spleen, muscle, and bone. In the heart, stomach, brain, and lung, tracer decreased rapidly after rapid increasing. Similarly, tracer uptake in the kidney and urinary bladder increased gradually. [^{68}Ga]Ga-FAPI-04 showed a rapid increasing and rapid decreasing trend in brain, lung, liver, spleen, bone, heart, kidney, and stomach. The mean effective dose of [^{68}Ga]Ga-PSMA-11 was 1.47E–02 mSv/MBq, and the mean effective doses of [^{18}F]F-FDG and [^{68}Ga]Ga-FAPI-04 were comparable (2.52E–02 mSv/MBq and 2.23E–02 mSv/MBq). The mean effective dose of [^{18}F]F-FDG was lower than that reported in the literature measured by previous short-axis PET, while both [^{68}Ga]Ga-PSMA-11 and [^{68}Ga]Ga-FAPI-04 had higher value than previously reported value.

Conclusions: [^{18}F]F-FDG, [^{68}Ga]Ga-PSMA-11 and [^{68}Ga]Ga-FAPI-04 have good biodistribution in human organs. Real-time high-sensitivity dynamic scanning with total-body PET/CT is a very effective way to accurately calculate biodistribution and effective dose of positron-labeled radiopharmaceuticals.

Keywords: Total-body positron emission tomography/computed tomography (total-body PET/CT); [^{18}F]F-FDG; [^{68}Ga]Ga-PSMA-11; [^{68}Ga]Ga-FAPI-04; biodistribution; dosimetry

Submitted Dec 23, 2022. Accepted for publication Jun 05, 2023. Published online Jun 21, 2023.
doi: 10.21037/qims-22-1418
View this article at: https://dx.doi.org/10.21037/qims-22-1418

Introduction

Molecular imaging with positron emission tomography (PET) has greatly improved clinical management of human diseases, especially cancers (1). PET is a molecular imaging technique with unparalleled specificity and sensitivity. The specificity of PET imaging comes from the specific PET tracers prepared by radiochemical methods, and the use of these tracers is the key to demonstrate the power and versatility of PET imaging. PET tracers are bioactive compounds labeled with positron emission radionuclides that interact with specific proteins, enzymes, or biochemical processes in the body. PET imaging collects and visualizes information about these interactions to explore physiology, pharmacology, causes of disease, and therapeutic mechanisms in living systems. There are many tracers currently used in clinic setting, among which [^{18}F] F-FDG, [^{68}Ga]Ga-PSMA-11, and [^{68}Ga]Ga-FAPI-04 are the most prominent tracers. [^{18}F]F-FDG plays an important role in evaluating disease staging of various malignancies, detecting early disease recurrence, evaluating treatment response, predicting prognosis, and assessing the spread of inflammatory diseases (2). [^{68}Ga]Ga-PSMA-11 has high sensitivity for prostate cancer imaging. Several studies have shown that the detection rate of [^{68}Ga]Ga-PSMA-11 PET/CT is higher than that of conventional imaging methods (3,4). In parallel, [^{68}Ga]Ga-FAPI-04 PET/CT showed good pharmacokinetics *in vivo* and was applied in the characterization of different types of tumors (5,6). However, a head-to-head comparison of dynamic circulation, distribution, and uptake patterns as well as radiation doses for these three representative tracers is lacking. With traditional short-axis PET/CT scanners, it was unable to fulfill the tasks.

With the joint efforts of experts from multiple tertiary hospitals, we have published the first version of consensus reporting the advantageous applications of the uExplorer PET/CT (7). The uExplorer PET/CT has the advantages of an ultra-long axial field of view (FOV), ultra-high resolution and sensitivity, this heavy-duty large device allows us to see and know more than the fast PET/CT scans. Compared to conventional scanners, uExplorer has a 40× increase in total-body imaging sensitivity, a 6.3× increase in single organ signal-to-noise ratio (SNR), and significant improvements in target-to-background ratio (TBR) and contrast-to-noise ratio (CNR). Due to the comprehensive improvement of the software and hardware, quantitative analysis of total-body PET/CT is more accurate, and image quality is more optimized (8,9).

We aimed to use total-body uExplorer scanner in real-time dynamic mode, rather than traditional short-axis (15–30 cm axial FOV length) scanning, to achieve realistic and dynamic observations of the systemic biodistribution of multiple tracers and to calculate precise radiation doses. Besides its importance in radiation assessment, it also helps to optimize injection doses, compare differences in radionuclides, observe biodistribution characteristics of different drugs labeled with the same radionuclide, improve image quality, and simplify clinical workflow.

Methods

Radiopharmaceutical preparation

[^{18}F]F-FDG, [^{68}Ga]Ga-PSMA-11 and [^{68}Ga]Ga-FAPI-04 were synthesized by Department of Nuclear Medicine, Renji Hospital, Shanghai Jiao Tong University following the standard protocols (10-12).

Patient recruitment and characteristics

A total of 54 patients undergoing total-body PET/CT were retrospectively included in the study, including 30 patients with [^{18}F]F-FDG, 10 patients with [^{68}Ga]Ga-PSMA-11, and 14 patients with [^{68}Ga]Ga-FAPI-04. The study was conducted in accordance with the Declaration of Helsinki (as revised in 2013). The study was approved by ethics board of Renji Hospital, School of Medicine, Shanghai Jiao Tong University and informed consent was taken from all the patients.

Total-body PET/CT scanning protocol

All 54 patients underwent dynamic scanning of whole body for 60 minutes using a total-body PET/CT scanner (uExplorer, United Imaging Healthcare) (13). History and physical examination were performed prior to PET/CT examination and all patients were asked to urinate before examination to ensure relative comfort during examination. For individual scanning, the patient was comfortably supine on the examination mattress during dynamic acquisition to achieve optimal imaging position and avoid motion artifacts. The CT scan tube voltage was 120 kV, and the dose was adjusted by automatic mas technology (14). Simultaneous PET acquisition was performed when the tracer was injected at the bedside, and maximum PET FOV was 194 cm.

Table 1 Characteristics of the included patients

Characteristics	[^{18}F]F-FDG	[^{68}Ga]Ga-PSMA-11	[^{68}Ga]Ga-FAPI-04
Age (years)	56.9 [28, 76]	66.2 [56, 78]	49.5 [36, 63]
Height (m)	1.67 [1.51, 1.83]	1.72 [1.65, 1.83]	1.68 [1.55, 1.8]
Weight (kg)	64.3 [40, 88]	73.6 [63, 93]	56.82 [41, 74]
Body mass index (kg/m^2)	22.87 [16.02, 32.05]	24.85 [22.06, 27.77]	20.21 [16.42, 27.64]
Injected dose (MBq)	285.1 [206.6, 373.3]	153.5 [124.3, 202.1]	118.5 [94.46, 154.9]
Injected dose per kg (MBq/kg)	4.48 [3.56, 6.36]	2.1 [1.8, 2.65]	2.1 [1.75, 3.1]
Patients	30	10	14

The values were presented as mean [range].

The PET raw data was reconstructed into 92 frames (24×5 s, 20×30 s, 48×60 s), and reconstruction parameters included standard ordered subset expectation maximization (OSEM) algorithm, time-of-flight (TOF), point-spread function (PSF) algorithms, 3 iterations, 20 subsets, 256×256 matrix, 600 mm FOV, 2.886 mm slice thickness, Gaussian post-filter with 3 mm full width at half maximum (FWHM). In addition, PET reconstruction incorporated standard corrections such as attenuation, scattering, randomization, dead time, and normalization.

Whole-body time-activity curves

Senior and experienced nuclear medicine physicians (W Wei and J Liu) used Pmod4.0 software (PMOD 4.0 Fusion, PMOD Technologies LLC, Zurich, Switzerland) (15) to quantitatively analyze the dynamic sequence of 92 frames. Taking into account the partial volume effect, the delineated volume of interest (VOI) was slightly smaller than the actual size of the organ. Tracer kinetics and cumulative organ activity were calculated using VOI to generate time-activity curves to visualize changes in subject's organ uptake and calculate internal radiation dose (16). Data and time-activity curves of heart were derived from the left ventricle.

Radiation effective dose estimates

Organ time-activity curves (TACs) were analyzed by PET using PMOD (Kinetic Modeling Module). The software calculated the trapezoidal integral over 60 minutes to obtain the organ cumulative activity (Bq-hr/Bq). The isotope tail was checked by pmod using the radioactive decay shape for the integration from the end of the last frame to infinity. Effective doses and individual organ doses were calculated for each patient using standard organ volumes with the OLINDA/EXM (version OLINDA/EXM 1.0, Vanderbilt University, Nashville, TN, USA) (17). The bladder wall had dynamic characteristics, and the interval between bladder urination was assumed to be two hours.

Results

Patient characteristics

The patient data are shown in *Table 1*. History and physical examination were performed prior to PET/CT examination, and all patients were asked to urinate before examination to ensure relative comfort during examination.

Biodistribution and radiation dose calculation

Representative whole-body PET/CT images of the three tracers at different time points are shown in *Figures 1-3*. *Figures 1-3* show the maximum intensity projection (MIP) images of [^{18}F]F-FDG, [^{68}Ga]Ga-PSMA-11, and [^{68}Ga]Ga-FAPI-04, respectively.

Consistent [^{18}F]F-FDG biodistribution was observed in all major organs of 30 patients, and TAC analysis results are shown in *Figure 4* and *Table 2*. The peak activity concentrations from high to low were urinary bladder, heart, kidney, spleen, liver, brain, stomach, lung, muscle, bone. Tracer uptake in muscle, stomach and bone showed a trend of rapid increase and steady uptake (*Figure 4A*). Among them, the activity concentration of muscle was the highest (3.10E+06±7.30E+05 kBq/cc), and the time to plateau in stomach was the shortest (7.92E+02±1.18E+03 s). Rapid increase of the tracer followed by rapid decrease in heart, kidney, liver, lung, and spleen was observed

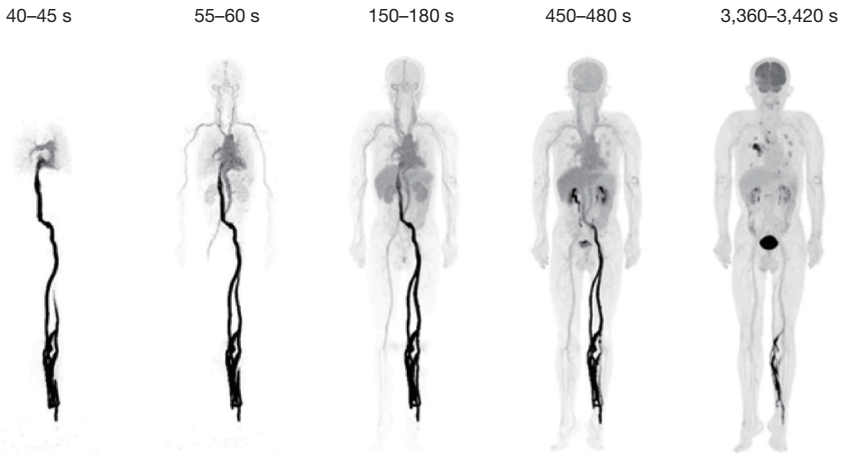

Figure 1 Whole body maximum intensity projection of [^{18}F]F-FDG. 40–45 s, pulmonary circulation distribution; 55–60 s, circulation distribution throughout the body; 150–180 s, tumor and multiple bone fracture uptake; 450–480 s, urinary bladder excretion; 3,360–3,420 s, tumor and multiple bone fracture concentration.

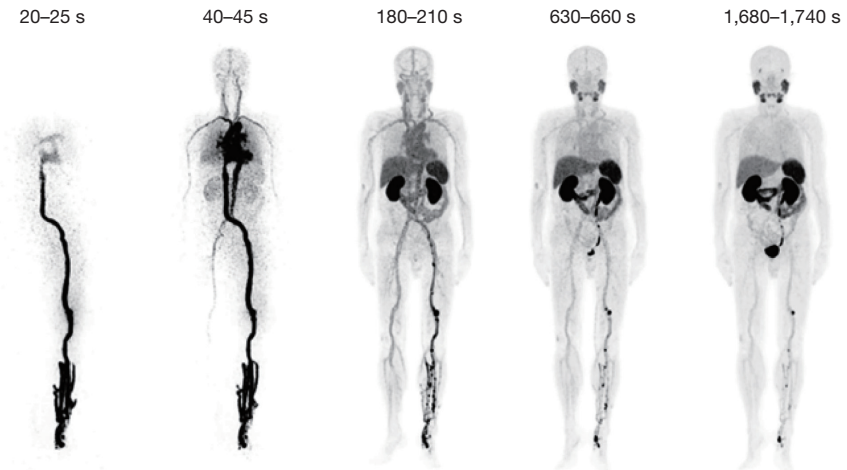

Figure 2 Whole body maximum intensity projection of [^{68}Ga]Ga-PSMA-11. 20–25 s, distribution of pulmonary circulation; 40–45 s, circulation distribution throughout the body; 180–210 s, imaging of parotid and submandibular glands; 630–660 s, imaging of urinary bladder; 1,680–1,740 s, decreased pulmonary circulation.

(*Figure 4B*). Peak times were similar for heart and lung (7.35E+01±6.65E+01 and 9.43E+01±1.17E+02 s), while stomach had the shortest peak time (7.92E+02±1.18E+03 s). The maximum activity concentration of liver and spleen were 2.69E+07±6.93E+06 kBq/cc and 2.85E+07±1.14E+07 kBq/cc, respectively. Brain and urinary bladder had similar TAC patterns, which were gradually increasing (*Figure 4C,4D*). Urinary bladder initially had no tracer uptake due to limited renal clearance at early time points. During 60 minutes of dynamic collection, tracer uptake in the brain and bladder continued to increase.

The results of TAC analysis of [^{68}Ga]Ga-PSMA-11 biodistribution in major organs of 10 patients are shown in *Figure 5* and *Table 3*. The peak activity concentrations from high to low were urinary bladder, kidney, heart, submandibular gland, spleen, parotid gland, liver, stomach, lung, muscle, brain, bone. Tracer uptake in liver, spleen, muscle and bone showed a trend of rapid increase and slow decrease (*Figure 5A,5B*). Among them, spleen had the highest peak activity concentration (1.73E+07±5.14E+06 kBq/cc),

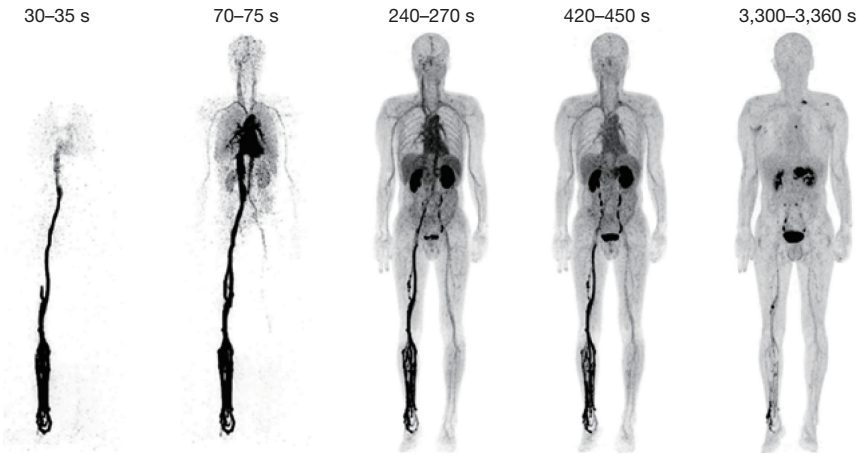

Figure 3 Whole body maximum intensity projection of [^{68}Ga]Ga-FAPI-04. 30–35 s, distribution of pulmonary circulation; 70–75 s, circulation distribution throughout the body; 240–270 s, urinary bladder imaging; 420–450 s, tumor concentration; 3,300–3,360 s, decreased renal uptake.

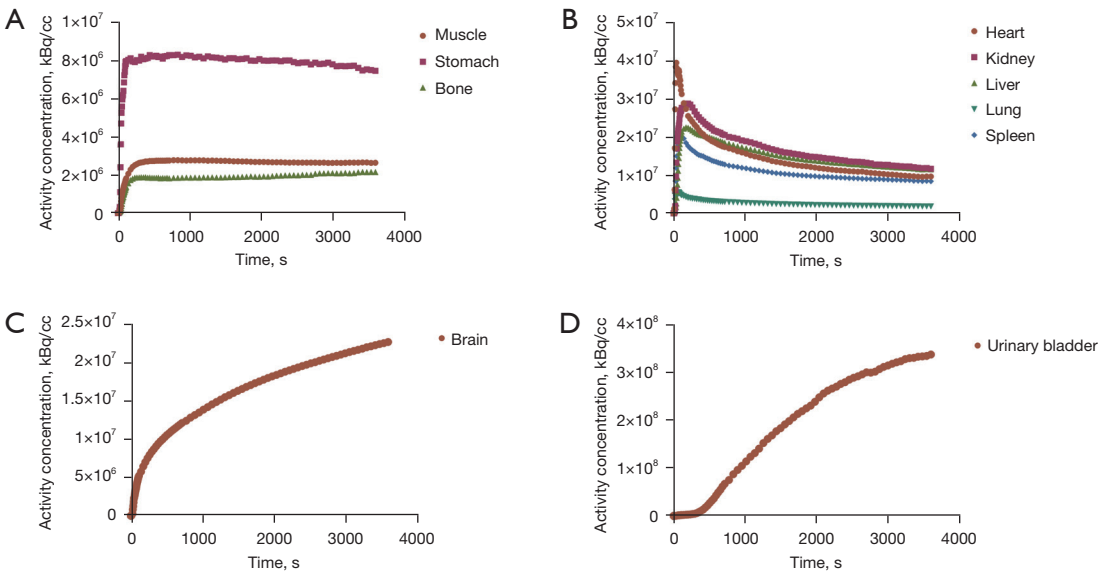

Figure 4 TAC curves of [^{18}F]F-FDG in major organs, including muscle, stomach and bone (A), heart, kidney, liver, lung and spleen (B), brain (C), urinary bladder (D). TAC, time-activity curve.

and bone had the shortest peak time (4.32E+02±1.77E+02 s). Rapid uptake of tracer followed by a rapid decrease occurred in the heart, stomach, brain and lung (*Figure 5C,5D*). Peak times of heart and lung were similar (6.15E+01±2.32E+01 and 6.20E+01±2.35E+01 s), while brain had the lowest peak activity concentration (9.73E+05±3.72E+05 kBq/cc). Tracer uptake in the kidney and urinary bladder was gradually increased (*Figure 5E*), with no uptake in the early stage of urinary bladder, a trend of fast uptake in the early stage of the kidney, and a fast uptake rate in the late stage of urinary bladder. Uptake patterns in the parotid and submandibular glands increased gradually over time (*Figure 5F*), and its peak time was close to urinary bladder. The peak of parotid gland was close to spleen. From the dynamic uptake patterns of parotid and submandibular glands shown in *Figure 5F*, it appears that vitamin C administration at an early time point or controlled release of vitamin C over the acquisition time may better decrease the accumulation of [^{68}Ga]Ga-PSMA-11

Table 2 Time-activity curves of [^{18}F]F-FDG in the main organs

TAC curve pattern	Organ	Time of peak arrival (s)	Peak activity concentration (kBq/cc)
Rapid increasing and steady uptaking	Muscle	1.22E+03±1.27E+03	3.10E+06±7.30E+05
	Stomach	7.92E+02±1.18E+03	1.14E+07±4.28E+06
	Bone	2.08E+03±1.53E+03	2.46E+06±1.94E+06
Rapid increasing and rapid decreasing	Heart	7.35E+01±6.65E+01	7.10E+07±3.87E+07
	Kidney	1.87E+02±1.93E+02	3.51E+07±1.16E+07
	Liver	2.29E+02±2.03E+02	2.69E+07±6.93E+06
	Lung	9.43E+01±1.17E+02	1.08E+07±7.23E+06
	Spleen	1.40E+02±1.41E+02	2.85E+07±1.14E+07
Gradually increasing	Brain	3.60E+03±0.00E+00	2.28E+07±5.58E+06
	Urinary bladder	3.38E+03±3.77E+02	3.53E+08±2.23E+08

The values were presented as mean ± SD. TAC, time-activity curve.

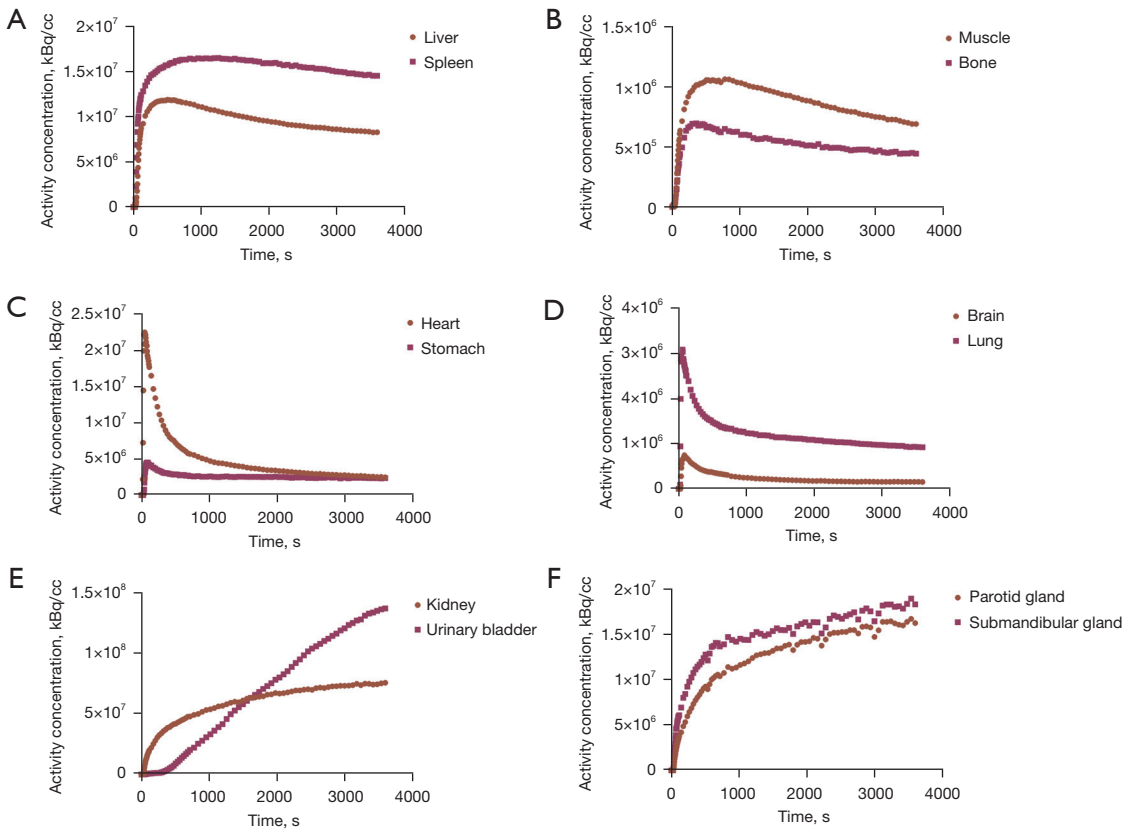

Figure 5 TAC curves of [^{68}Ga]Ga-PSMA-11 in the major organs, including liver and spleen (A), muscle and bone (B), heart and stomach (C), brain and lung (D), kidney and urinary bladder (E), parotid gland and submandibular gland (F). TAC, time-activity curve.

Table 3 Time-activity curves of [^{68}Ga]Ga-PSMA-11 in the main organs

TAC curve pattern	Organ	Time of peak arrival (s)	Peak activity concentration (kBq/cc)
Rapid increasing and slow decreasing	Liver	5.28E+02±9.08E+01	1.20E+07±2.70E+06
	Spleen	8.32E+02±4.92E+02	1.73E+07±5.14E+06
	Muscle	6.75E+02±3.22E+02	1.10E+06±2.03E+05
	Bone	4.32E+02±1.77E+02	7.44E+05±2.59E+05
Rapid increasing and rapid decreasing	Heart	6.15E+01±2.32E+01	3.06E+07±1.40E+07
	Stomach	5.51E+02±9.64E+02	5.47E+06±3.49E+06
	Brain	7.90E+01±2.91E+01	9.73E+05±3.72E+05
	Lung	6.20E+01±2.35E+01	4.31E+06±2.16E+06
Gradually increasing	Kidney	3.19E+03±6.87E+02	7.70E+07±3.25E+07
	Urinary bladder	3.49E+03±2.17E+02	1.40E+08±5.83E+07
	Parotid gland	3.49E+03±1.43E+02	1.71E+07±3.90E+06
	Submandibular gland	3.38E+03±2.61E+02	1.96E+07±6.66E+06

The values were presented as mean ± SD. TAC, time-activity curve.

in the parotid and submandibular glands. The hypothesis needs to be validated in future studies.

The results of TAC analysis of [^{68}Ga]Ga-FAPI-04 biodistribution in major organs of 14 patients are shown in *Figure 6* and *Table 4*. The peak activity concentrations from high to low were urinary bladder, heart, kidney, spleen, liver, stomach, lung, muscle, brain, bone. Tracer uptake in brain, lung, liver, spleen, bone, heart, kidney, and stomach showed a trend of rapid increase and rapid decrease (*Figure 6A-6C*). Heart had the highest peak activity concentration (3.15E+07±1.43E+07 kBq/cc). Peak times of heart and lung are similar (5.46E+01±2.52E+01 and 5.54E+01±2.66E+01 s). Brain and bone had lower peak activity concentrations (1.39E+06±6.22E+05 and 1.36E+06±5.46E+05 kBq/cc). In muscle, there was a rapid uptake of the tracer followed by a slow decrease (*Figure 6D*). The uptake trend of urinary bladder was consistent with that of [^{18}F]F-FDG, with no uptake in the initial stage and a gradual increase at the later stage (*Figure 6E*).

Effective doses of various tracers in organs of interest were calculated using the OLINDA/EXM software. *Table 5* shows the standardized cumulated activity values of multiple tracer organs. It can be seen from *Table 6* that effective radiation dose of [^{68}Ga]Ga-PSMA-11 is the lowest (1.47E–02±2.27E–03 mSv/MBq), and the mean effective dose is slightly higher than that of ^{18}F-PSMA-11 (1.28E–02 mSv/MBq) reported by Piron *et al.* (18). The effective doses of [^{18}F]F-FDG and [^{68}Ga]Ga-FAPI-04 were similar (2.52E–02±1.04E–02 and 2.23E–02±7.29E–03 mSv/MBq). The difference in the mean effective dose is that the radiation dose of [^{18}F]F-FDG is lower than that reported by Deloar *et al.* (2.9E–02 mSv/MBq) (19), and the effective dose of [^{68}Ga]Ga-FAPI-04 is higher than that reported by Giesel *et al.* (1.64E–02 mSv/MBq) (5). The injection dose of [^{18}F]F-FDG (285.1±43.74 MBq) was the highest, partially resulted in the highest internal radiation dose in a single examination.

Discussion

Total-body PET/CT has a long field of view and a wider detection angle, which is 40 times more sensitive than the traditional short-axis PET/CT. High-sensitivity and rapid scanning provide the opportunity to suppress motility of the gastrointestinal tract, making the fusion of PET and CT more accurate (20,21). Total-body uninterrupted continuous dynamic scanning is beneficial for simultaneous analysis of total-body pharmacokinetics of radiotracers and radioligands. Moreover, the calculated radiation dose is more accurate.

Based on 1-hour uninterrupted TAC analysis, [^{68}Ga]Ga-PSMA-11 and [^{68}Ga]Ga-FAPI-04 showed the same uptake trends in brain, lung, heart, stomach, and bone, but different uptake trends in other organs. The

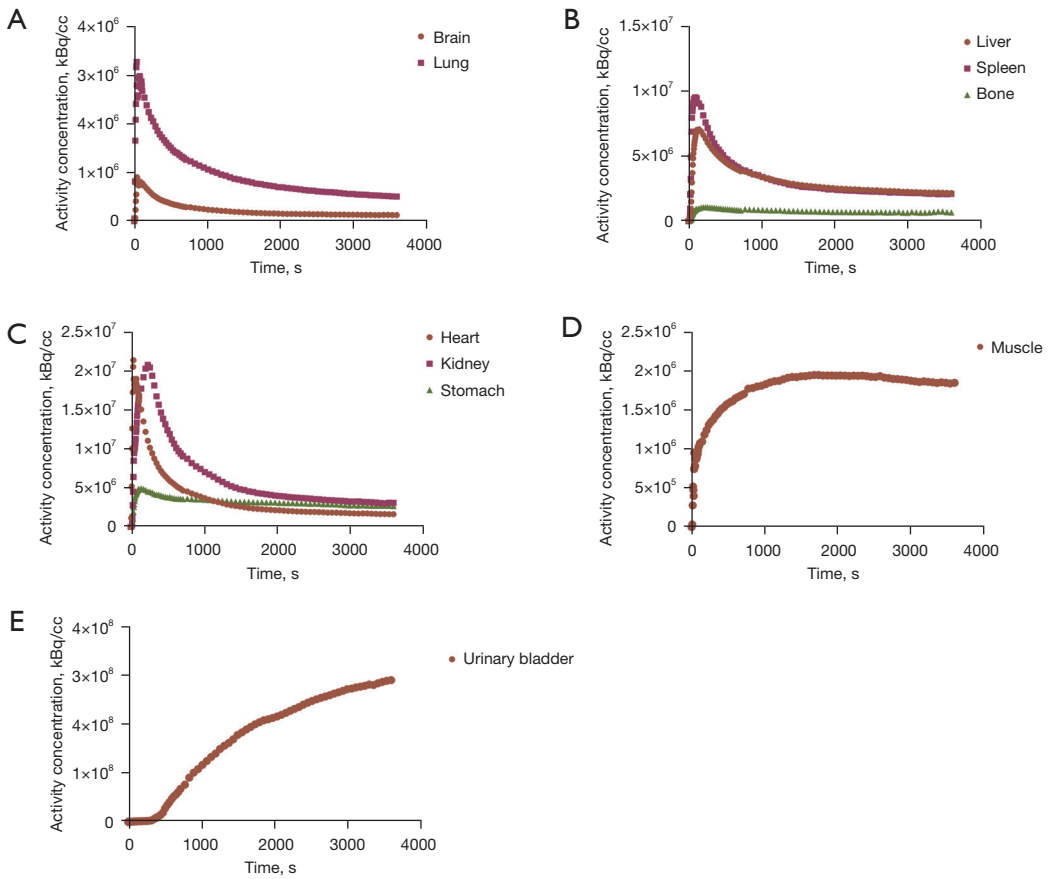

Figure 6 TAC curves of [^{68}Ga]Ga-FAPI-04 in the major organs, including brain and lung (A), liver, spleen and bone (B), heart, kidney and stomach (C), muscle (D), urinary bladder (E). TAC, time-activity curve.

Table 4 Time-activity curves of [68Ga]Ga-FAPI-04 in the main organs.

TAC curve pattern	Organ	Time of peak arrival (s)	Peak activity concentration (kBq/cc)
Rapid increasing and rapid decreasing	Brain	6.57E+01±2.79E+01	1.39E+06±6.22E+05
	Lung	5.54E+01±2.66E+01	5.20E+06±2.59E+06
	Liver	1.58E+02±9.12E+01	8.17E+06±2.31E+06
	Spleen	1.06E+02±5.74E+01	1.20E+07±4.28E+06
	Bone	6.60E+02±9.78E+02	1.36E+06±5.46E+05
	Heart	5.46E+01±2.52E+01	3.15E+07±1.43E+07
	Kidney	2.94E+02±1.97E+02	2.22E+07±7.88E+06
	Stomach	5.53E+02±1.11E+03	6.11E+06±3.11E+06
Rapid increasing and slow decreasing	Muscle	1.84E+03±1.03E+03	2.67E+06±1.37E+06
Gradually increasing	Urinary bladder	3.58E+03±2.98E+01	2.92E+08±1.32E+08

The values were presented as mean ± SD. TAC, time-activity curve.

Table 5 Standardized cumulated activity for multiple tracers

Target organ	FDG	PSMA	FAPI
Brain	2.49E−01±6.60E−02	3.07E−03±8.08E−04	3.02E−03±8.40E−04
Heart contents	4.37E−02±7.64E−03	1.73E−02±2.35E−03	1.53E−02±2.37E−03
Kidneys	3.40E−02±6.17E−03	2.07E−01±7.92E−02	1.79E−02±3.42E−03
Liver	1.92E−01±2.62E−02	1.75E−01±5.01E−02	5.97E−02±3.52E−02
Lungs	1.68E−02±2.95E−03	1.10E−02±2.22E−03	8.58E−03±1.64E−03
Muscle	5.59E−01±1.22E−01	2.23E−01±3.36E−02	6.03E−01±1.57E−01
Trabecular bone	1.66E−02±1.16E−02	4.98E−03±1.33E−03	8.55E−03±2.73E−03
Spleen	1.40E−02±1.76E−03	2.78E−02±8.86E−03	5.79E−03±1.43E−03
Urinary bladder contents	4.99E−01±3.27E−01	2.24E−01±9.04E−02	5.56E−01±2.27E−01
Remainder	7.49E−01±4.23E−01	5.40E−01±1.77E−01	1.49E−01±2.50E−01

The values were presented as mean ± SD. FDG, [^{18}F]F-FDG; PSMA, [^{68}Ga]Ga-PSMA-11; FAPI, [^{68}Ga]Ga-FAPI-04.

Table 6 Radiation dose estimations for multiple tracers (mSv/MBq)

Target organ	FDG	PSMA	FAPI
Adrenals	5.04E−05±1.15E−05	3.10E−05±7.95E−06	2.34E−05±7.30E−06
Brain	2.28E−04±6.43E−05	4.50E−06±1.48E−06	6.26E−06±1.85E−06
Breasts	2.74E−04±1.01E−04	1.73E−04±3.18E−05	1.05E−04±6.35E−05
LLI wall	1.8E−03±4.37E−04	9.08E−04±1.16E−04	1.44E−03±3.46E−04
Small intestine	5.39E−05±8.49E−06	2.31E−05±8.87E−06	3.36E−05±7.67E−06
Stomach wall	1.02E−03±2.9E−04	7.82E−04±7.06E−05	4.82E−04±1.84E−04
ULI wall	5.25E−05±1.03E−05	2.26E−05±8.46E−06	3.01E−05±7.49E−06
Kidneys	1.38E−04±2.29E−05	2.78E−03±1.81E−03	7.34E−05±8.55E−06
Liver	1.51E−03±1.95E−04	1.24E−03±3.01E−04	5.21E−04±1.92E−04
Lungs	1.02E−03±1.77E−04	6.25E−04±5.11E−05	5.36E−04±1.41E−04
Muscle	5.10E−05±7.10E−06	1.65E−05±6.28E−06	4.37E−05±8.17E−06
Ovaries	2.97E−03±6.82E−04	1.53E−03±1.73E−04	2.35E−03±5.58E−04
Pancreas	5.14E−05±1.21E−05	2.95E−05±8.35E−06	2.39E−05±7.78E−06
Red marrow	1.08E−03±1.78E−04	6.52E−04±4.74E−05	5.62E−04±1.31E−04
Osteogenic cells	1.20E−04±3.13E−05	6.35E−05±1.11E−05	4.99E−05±2.15E−05
Skin	5.66E−05±1.40E−05	3.28E−05±4.74E−06	2.78E−05±9.13E−06
Spleen	1.04E−04±1.32E−05	1.08E−04±4.37E−05	4.85E−05±1.02E−05
Thymus	3.75E−05±1.13E−05	1.36E−05±5.55E−06	1.74E−05±7.34E−06
Thyroid	3.40E−04±1.01E−04	1.77E−04±3.94E−05	1.45E−04±6.39E−05
Urinary bladder wall	1.42E−02±9.69E−03	5.48E−03±2.11E−03	1.57E−02±6.70E−03
Uterus	1.17E−04±4.24E−05	3.87E−05±2.06E−05	1.07E−04±3.07E−05
Effective dose	2.52E−02±1.04E−02	1.47E−02±2.27E−03	2.23E−02±7.29E−03

The values were presented as mean ± SD. FDG, [^{18}F]F-FDG; PSMA, [^{68}Ga]Ga-PSMA-11; FAPI, [^{68}Ga]Ga-FAPI-04; LLI, lower large intestine; ULI, upper large intestine.

internal radiation doses of the same radionuclide-labeled PSMA (1.47E–02±2.27E–03 mSv/MBq) and FAPI (2.23E–02±7.29E–03mSv/MBq) are quite different, and the difference may be internal (such as the properties of the precursors and the associated pharmacokinetics) or externally (such as differences in injection doses of the radiopharmaceuticals) (22). The injection dose of [^{18}F]F-FDG was the highest (285.1±43.74 MBq), and the total internal radiation dose in a single examination was higher than that of [^{68}Ga]Ga-PSMA-11 and [^{68}Ga]Ga-FAPI-04. [^{68}Ga]Ga-PSMA-11 had the lowest radiation dose (1.47E–02±2.27E–03 mSv/MBq), and the mean effective dose was slightly higher than that of Piron *et al.* (1.28E–02 mSv/MBq) (18). The possible reason was that different nuclide markers resulted in different cumulative activity of organs. The article reported that oral administration of vitamin C decreased [^{68}Ga]Ga-PSMA-11 accumulation in salivary glands during examination (23). In the study by Yu *et al.*, vitamin C was given 30 min after starting the dynamic PET acquisition (23). Radiation doses of [^{18}F]F-FDG and [^{68}Ga]Ga-FAPI-04 were comparable (2.52E–02±1.04E–02 mSv/MBq and 2.23E–02±7.29E–03 mSv/MBq), the effective dose of [^{18}F]F-FDG was close to that reported in the literature (24). The corresponding dose of [^{68}Ga]Ga-FAPI-04 was higher than that reported by Giesel *et al.* (1.64E–02 mSv/MBq) (5). In the literature, fitting functions were used for integration from the last measured point in time to infinity instead of using the radioactive decay shape for the integration. The mean effective dose of [^{18}F]F-FDG was lower than that reported by Deloar *et al.* (2.9E–02 mSv/MBq) (19), total-body dynamic acquisition provided more realistic biological distribution data, and the calculated shorter retention time resulted in a lower calculated effective dose. Compared to Fluorine-18 (^{18}F), gallium-68 (^{68}Ga) has a relatively high positron energy, resulting in a large number of image quality degradations. In addition, the presence of statistical noise further degrades image quality. The difference of reconstruction methods will also affect the image quality (25). From the subjective point of view of image quality, the image noise of ^{18}F-labeled FDG is lower than that of ^{68}Ga-labeled PSMA and FAPI (26).

Previous studies of these three tracers lacked a macroscopic and systematic interpretation of the biodistribution of whole-body organs, and the main limitation was that multi-bed PET/CT scans could not truly study whole body biodistribution and radiation dose of the tracers (19,24,27); the missing of multiple time points for some organs leading to biases in subsequent dose estimates. Short-axis PET/CT can design different single-bed scan time according to the peak time of the three tracers. This enables faster scanning of multiple organs throughout the body and avoids the loss of peak data for some organs. At present, there is no literature reporting radiation dose of [^{68}Ga]Ga-FAPI-04 and [^{68}Ga]Ga-PSMA-11 calculated by total-body PET/CT scanning. A more accurate description of the biodistribution profiles of [^{68}Ga]Ga-FAPI-04 and [^{68}Ga]Ga-PSMA-11 and the calculation of radiation dose will better guide radionuclide therapy. For instance, accurate dose assessment of [^{68}Ga]Ga-PSMA could be of great value in further optimizing the clinical application of long half-life ^{177}Lu-labeled PSMA inhibitors (e.g., [^{177}Lu]Lu-PSMA-617) (28).

One of the limitations of our study is the limited number of [^{68}Ga]Ga-PSMA-11 and [^{68}Ga]Ga-FAPI-04 dynamic scans, with only 10 and 14 cases, respectively. More cases and volunteers will be recruited for in-depth and comprehensive research in the future. Another limitation is the lack of time points after 60 minutes, mainly due to the movement of the patient during long-term dynamic acquisitions, which affects the accuracy of the results, and more time points can be added to calculate more precise radiation dose estimation. In addition, the truncation artifact generated by the patient's hands on the sides of the body during dynamic scanning may interfere with the attenuation correction of PET images (29).

The effective dose of the radioactive tracer for a single PET imaging session was lower than 50 mSv per year established by the National Institutes of Health for this study (30), allowing for multiple PET scans per year of the same subject. In the future, we plan to achieve longer PET dynamic PET scan cycles in eligible healthy volunteers, combined with more time points to study whole-body biological distribution and radiation dose, and will consider larger sample sizes and subjects with different characteristics. In addition, biological distribution and dosimetry calculation of therapeutic radiopharmaceuticals remains to be explored in the future studies. Finally, we also analyzed indications and diagnostic performance of total-body dynamic PET/CT scanning using the above three radioactive tracers, simplifying the clinical workflows and improving the diagnostic performances.

Conclusions

Through total-body uninterrupted dynamic PET/CT

scanning, we observed that [^{18}F]F-FDG, [^{68}Ga]Ga-PSMA-11 and [^{68}Ga]Ga-FAPI-04 had good biodistribution in human organs and accurately calculated the corresponding effective doses. It will be helpful to optimize injection dose and simplify clinical workflow in the future studies. Short-axis PET/CT can optimize the dynamic acquisition scheme and static imaging time based on the biological distribution and peak time of multiple organs with different tracers, achieving more accurate pharmacokinetic analysis and clinical diagnosis.

Acknowledgments

The authors want to thank all the clinical and research staff at the Department of Nuclear Medicine, Renji Hospital, Shanghai Jiao Tong University for their technical assistance and helpful discussions.
Funding: This work was supported in part by the National Key Research and Development Program of China (Nos. 2020YFA0909000 and 2021YFA0910000), the National Natural Science Foundation of China (Nos. 82001878 and 82171972), and the Shanghai Rising-Star Program (No. 20QA1406100).

Footnote

Conflicts of Interest: All authors have completed the ICMJE uniform disclosure form (available at https://qims.amegroups.com/article/view/10.21037/qims-22-1418/coif). The authors have no conflicts of interest to declare.

Ethical Statement: The authors are accountable for all aspects of the work in ensuring that questions related to the accuracy or integrity of any part of the work are appropriately investigated and resolved. The study was conducted in accordance with the Declaration of Helsinki (as revised in 2013). The study was approved by ethics board of Renji Hospital, School of Medicine, Shanghai Jiao Tong University and informed consent was taken from all the patients.

References

1. Nerella SG, Singh P, Sanam T, Digwal CS. PET Molecular Imaging in Drug Development: The Imaging and Chemistry Perspective. Front Med (Lausanne) 2022;9:812270.
2. Ozaki K, Harada K, Terayama N, Kosaka N, Kimura H, Gabata T. FDG-PET/CT imaging findings of hepatic tumors and tumor-like lesions based on molecular background. Jpn J Radiol 2020;38:697-718.
3. Afshar-Oromieh A, Zechmann CM, Malcher A, Eder M, Eisenhut M, Linhart HG, Holland-Letz T, Hadaschik BA, Giesel FL, Debus J, Haberkorn U. Comparison of PET imaging with a (68)Ga-labelled PSMA ligand and (18)F-choline-based PET/CT for the diagnosis of recurrent prostate cancer. Eur J Nucl Med Mol Imaging 2014;41:11-20.
4. Perera M, Papa N, Roberts M, Williams M, Udovicich C, Vela I, Christidis D, Bolton D, Hofman MS, Lawrentschuk N, Murphy DG. Gallium-68 Prostate-specific Membrane Antigen Positron Emission Tomography in Advanced Prostate Cancer-Updated Diagnostic Utility, Sensitivity, Specificity, and Distribution of Prostate-specific Membrane Antigen-avid Lesions: A Systematic Review and Meta-analysis. Eur Urol 2020;77:403-17.
5. Giesel FL, Kratochwil C, Lindner T, Marschalek MM, Loktev A, Lehnert W, Debus J, Jäger D, Flechsig P, Altmann A, Mier W, Haberkorn U. (68)Ga-FAPI PET/CT: Biodistribution and Preliminary Dosimetry Estimate of 2 DOTA-Containing FAP-Targeting Agents in Patients with Various Cancers. J Nucl Med 2019;60:386-92.
6. Lindner T, Loktev A, Altmann A, Giesel F, Kratochwil C, Debus J, Jäger D, Mier W, Haberkorn U. Development of Quinoline-Based Theranostic Ligands for the Targeting of Fibroblast Activation Protein. J Nucl Med 2018;59:1415-22.
7. Yu H, Gu Y, Fan W, Gao Y, Wang M, Zhu X, Wu Z, Liu J, Li B, Wu H, Cheng Z, Wang S, Zhang Y, Xu B, Li S, Shi H. Expert consensus on oncological [18F]FDG total-body PET/CT imaging (version 1). Eur Radiol 2023;33:615-26.
8. Hu P, Lin X, Zhuo W, Tan H, Xie T, Liu G, Chen S, Chen X, Yu H, Zhang Y, Shi H, Liu H. Internal dosimetry in F-18 FDG PET examinations based on long-time-

measured organ activities using total-body PET/CT: does it make any difference from a short-time measurement? EJNMMI Phys 2021;8:51.
9. Cherry SR, Jones T, Karp JS, Qi J, Moses WW, Badawi RD. Total-Body PET: Maximizing Sensitivity to Create New Opportunities for Clinical Research and Patient Care. J Nucl Med 2018;59:3-12.
10. Chen H, Pang Y, Wu J, Zhao L, Hao B, Wu J, Wei J, Wu S, Zhao L, Luo Z, Lin X, Xie C, Sun L, Lin Q, Wu H. Comparison of [68Ga]Ga-DOTA-FAPI-04 and [18F] FDG PET/CT for the diagnosis of primary and metastatic lesions in patients with various types of cancer. Eur J Nucl Med Mol Imaging 2020;47:1820-32.
11. Demirci E, Sahin OE, Ocak M, Akovali B, Nematyazar J, Kabasakal L. Normal distribution pattern and physiological variants of 68Ga-PSMA-11 PET/CT imaging. Nucl Med Commun 2016;37:1169-79.
12. Wen J, Zhu Y, Li L, Liu J, Chen Y, Chen R. Determination of optimal (68) Ga-PSMA PET/CT imaging time in prostate cancers by total-body dynamic PET/CT. Eur J Nucl Med Mol Imaging 2022;49:2086-95.
13. Badawi RD, Shi H, Hu P, Chen S, Xu T, Price PM, Ding Y, Spencer BA, Nardo L, Liu W, Bao J, Jones T, Li H, Cherry SR. First Human Imaging Studies with the EXPLORER Total-Body PET Scanner. J Nucl Med 2019;60:299-303.
14. Hsiao IT, Lin KJ, Huang KL, Huang CC, Chen HS, Wey SP, Yen TC, Okamura N, Hsu JL. Biodistribution and Radiation Dosimetry for the Tau Tracer (18)F-THK-5351 in Healthy Human Subjects. J Nucl Med 2017;58:1498-503.
15. Sah BR, Sommerauer M, Mu L, Gonzalez GP, Geistlich S, Treyer V, Schibli R, Buck A, Warnock G, Ametamey SM. Radiation dosimetry of [18F]-PSS232-a PET radioligand for imaging mGlu5 receptors in humans. EJNMMI Res 2019;9:56.
16. Demir M, Toklu T, Abuqbeitah M, Çetin H, Sezgin HS, Yeyin N, Sönmezo lu K. Evaluation of PET Scanner Performance in PET/MR and PET/CT Systems: NEMA Tests. Mol Imaging Radionucl Ther 2018;27:10-8.
17. Stabin MG, Sparks RB, Crowe E. OLINDA/EXM: the second-generation personal computer software for internal dose assessment in nuclear medicine. J Nucl Med 2005;46:1023-7.
18. Piron S, De Man K, Van Laeken N, D'Asseler Y, Bacher K, Kersemans K, Ost P, Decaestecker K, Deseyne P, Fonteyne V, Lumen N, Achten E, Brans B, De Vos F. Radiation Dosimetry and Biodistribution of (18) F-PSMA-11 for PET Imaging of Prostate Cancer. J Nucl Med 2019;60:1736-42.
19. Deloar HM, Fujiwara T, Shidahara M, Nakamura T, Watabe H, Narita Y, Itoh M, Miyake M, Watanuki S. Estimation of absorbed dose for 2-[F-18]fluoro-2-deoxy-D-glucose using whole-body positron emission tomography and magnetic resonance imaging. Eur J Nucl Med 1998;25:565-74.
20. Zhang X, Cherry SR, Xie Z, Shi H, Badawi RD, Qi J. Subsecond total-body imaging using ultrasensitive positron emission tomography. Proc Natl Acad Sci U S A 2020;117:2265-7.
21. Zhang X, Zhou J, Cherry SR, Badawi RD, Qi J. Quantitative image reconstruction for total-body PET imaging using the 2-meter long EXPLORER scanner. Phys Med Biol 2017;62:2465-85.
22. Miller C, Rousseau J, Ramogida CF, Celler A, Rahmim A, Uribe CF. Implications of physics, chemistry and biology for dosimetry calculations using theranostic pairs. Theranostics 2022;12:232-59.
23. Yu H, Lv J, Hu P, Chen S, Shi H. Reduction of radiation accumulation in salivary glands through oral vitamin C during 68Ga-PSMA-11 total-body dynamic PET/CT imaging. Nucl Med Commun 2022;43:166-71.
24. Srinivasan S, Crandall JP, Gajwani P, Sgouros G, Mena E, Lodge MA, Wahl RL. Human Radiation Dosimetry for Orally and Intravenously Administered (18)F-FDG. J Nucl Med 2020;61:613-9.
25. Gao J, Liu Q, Zhou C, Zhang W, Wan Q, Hu C, Gu Z, Liang D, Liu X, Yang Y, Zheng H, Hu Z, Zhang N. An improved patch-based regularization method for PET image reconstruction. Quant Imaging Med Surg 2021;11:556-70.
26. Gavriilidis P, Koole M, Annunziata S, Mottaghy FM, Wierts R. Positron Range Corrections and Denoising Techniques for Gallium-68 PET Imaging: A Literature Review. Diagnostics (Basel) 2022.
27. Lizana H, Johansson L, Axelsson J, Larsson A, Ögren M, Linder J, Halldin C, Varrone A, Mo SJ. Whole-Body Biodistribution and Dosimetry of the Dopamine Transporter Radioligand (18)F-FE-PE2I in Human Subjects. J Nucl Med 2018;59:1275-80.
28. Jackson PA, Hofman MS, Hicks RJ, Scalzo M, Violet J. Radiation Dosimetry in (177)Lu-PSMA-617 Therapy Using a Single Posttreatment SPECT/CT Scan: A Novel Methodology to Generate Time- and Tissue-Specific Dose Factors. J Nucl Med 2020;61:1030-6.
29. Mawlawi O, Erasmus JJ, Pan T, Cody DD, Campbell R, Lonn AH, Kohlmyer S, Macapinlac HA, Podoloff DA.

Truncation artifact on PET/CT: impact on measurements of activity concentration and assessment of a correction algorithm. AJR Am J Roentgenol 2006;186:1458-67.

30. Kehoe T. International Commission on Radiological Protection publications 97 and 98: radiation protection can be fun! Clin Oncol (R Coll Radiol) 2007;19:539-41.

Cite this article as: Li L, Wan L, Zhao H, Wang C, Wei W, Liu J. Biodistribution and radiation dosimetry of multiple tracers on total-body positron emission tomography/computed tomography. Quant Imaging Med Surg 2023;13(8):5182-5194. doi: 10.21037/qims-22-1418

